Available online at www.sciencedirect.com
SCIENCE DIRECT®
ELSEVIER
International Journal of Machine Tools & Manufacture 44 (2004) 1413–1421
INTERNATIONAL JOURNAL OF MACHINE TOOLS & MANUFACTURE DESIGN, RESEARCH AND APPLICATION
www.elsevier.com/locate/ijmactool

An analytical finite element technique for predicting thrust force and torque in drilling

J.S. Strenkowski [a,*], C.C. Hsieh [a], A.J. Shih [b]

[a] Department of Mechanical and Aerospace Engineering, North Carolina State University, Raleigh, NC 27695-7910, USA
[b] Department of Mechanical Engineering, University of Michigan, Ann Arbor, MI 48109, USA

Received 3 January 2003; received in revised form 17 December 2003; accepted 18 January 2004

Abstract

An analytical finite element technique was developed for predicting the thrust force and torque in drilling with twist drills. The approach was based on representing the cutting forces along the cutting lips as a series of oblique sections. Similarly, cutting in the chisel region was treated as orthogonal cutting with different cutting speeds depending on the radial location. For each section, an Eulerian finite element model was used to simulate the cutting forces. The section forces were combined to determine the overall thrust force and drilling torque. Good agreement between the predicted and measured forces and torques was found in orthogonal and oblique cutting and in drilling tests. The drilling tests were performed on AISI 1020 for several drill diameters, spindle speeds, and feed rates. An extension of the technique for predicting drill temperatures has also been described.

Keywords: Finite element modeling; drilling; drilling thrust force and torque

1. Introduction

Metal cutting operations such as turning, milling and drilling are widely used in manufacturing to produce a variety of mechanical components. Drilling, a hole producing process, is especially important because it accounts for a large portion of overall machining operations. In addition, drilling problems can result in costly production waste because many drilling operations are usually among the final steps in fabricating a part.

Many analytical and numerical models have been developed by many researchers in the past 50 years [1–28] for predicting torque and thrust force in drilling. Early drilling models have been developed by Shaw [1], Oxford [2], Shaw and Oxford [3], Pal et al. [4], Williams [5,6], Armarego and Cheng [7,8], and Wiriyacosol and Armarego [9]. A methodology was presented by Armarego and Cheng [7,8] in which a series of oblique cutting slices was used to model the drilling process. This approach was further expanded by Watson [10–13] for more detailed modelling of material removal in both the cutting lip and chisel edge regions. Armarego's approach was also utilized by Agapiou and DeVries [14,15] to predict drill temperatures, and by Stephenson and Agapiou [16] to simulate arbitrary drill point geometries. In addition, Rubenstein [17,18] investigated the use of a spade drill model.

More recent developments in drilling models have utilized either a mechanistic or a finite element approach. Chandrasekarn et al. [19–21] and Gong and Ehmann [22] developed mechanistic drilling models. The finite element method can provide a unified approach for drilling and other metal cutting processes. Fuh [23] explored the use of the finite element method for drilling. Guo and Dornfeld [24] and Min et al. [25] applied the finite element technique for modeling drilling and exit burr formation. A finite element approach was used by Shatla and Altan [26] to determine drilling torque and thrust force, and by Bono and Ni [27,28] to predict drill heat flux, temperatures, and the thermal distortion of drill holes.

* Corresponding author. Tel.: +1-919-515-7950.
E-mail address: jsstren@eos.ncsu.edu (J.S. Strenkowski).

0890-6955/$ - see front matter © 2004 Published by Elsevier Ltd.
doi:10.1016/j.ijmachtools.2004.01.005

Nomenclature

A	Area in the shear plane
b	Cutting width
F_H	Principal (cutting) force
F_t	Friction force
F_T	Transverse force
F_V	Vertical (thrust) force
i	Inclination angle
L	Pitch of the helix on the drill
N_t	Normal force
Q	Projected area of the cutting cross section
r	Radius of the section from drill center
t	Undeformed chip thickness
t_1	Depth of cut
U_s	Shear energy rate
U_f	Friction energy rate
V	Cutting velocity
V_c	Chip flow velocity
V_s	Chip velocity in the shear plan
w	Half of the web thickness
α_e	Effective rake angle
α_n	Rake angle
β	Friction angle
ϕ_e	Shear plane angle, angle between the shear and cutting velocity
η_c	Chip flow angle
ρ	Half of the drill point angle
τ_s	Shear stress in the shear plane

In this paper, an Eulerian thermo-viscoplastic finite element model that has been developed for oblique cutting [29] was applied to the drilling process. The finite element cutting model was based on a series of research articles by Carroll and Strenkowski [30], Strenkowski and Moon [31], and Athavale and Strenkowski [32] and it has been validated for numerous workpiece materials and cutting conditions. The Eulerian finite element approach is particularly advantageous because it can be used to model chip formation with large negative rake angles as found in the chisel edge of a twist drill. Another unique feature was that both the forces and the heating of the drill due to plastic work and friction can be integrated in a single model to predict forces and drill temperatures as a function of workpiece, feed and speed.

In this paper, the development of a finite element drilling model is described. The model is based on representing the drill point geometry as a series of oblique sections. An analytical model for oblique cutting is first described for analyzing a single section in the cutting lip region of the drill. Results of these sections are then combined to determine the thrust force and torque for various operating conditions. The model is verified by comparing predicted thrust force and torque with measured and published data. An extension of the model for predicting drill temperatures is also discussed.

2. Single-edge oblique cutting model

The cutting action along the cutting lips in a drill can be interpreted as occurring within a series of oblique sections, in which the rake and inclination angles vary radially along each lip [7,8]. In this paper, an analytical finite element technique was adopted for predicting the chip flow angle and three-dimensional oblique cutting forces that occurs in each section [29]. The technique was based on a minimum energy approach as developed by Usui et al. [33] and Usui and Hirota [34] for determining the chip flow angle. An Eulerian model developed by Strenkowski et al. [29] was coupled with this minimum energy approach for the orthogonal cutting force data.

Consider first the simplest case of a tool with an oblique cutting edge as shown in Fig. 1, which has been adapted from Usui et al. [33]. The inclination angle of the main cutting edge is i, the depth of cut is

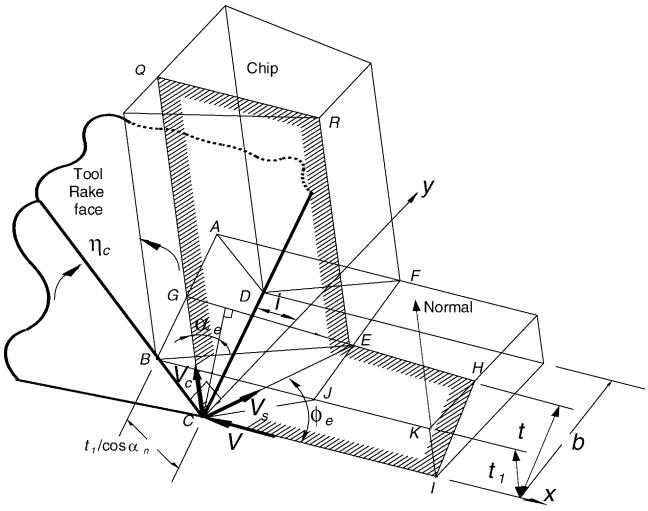

Fig. 1. Model of oblique cutting.

t_1, and the cutting width is b. The underlying assumption is that a chip is produced by shear forces acting in the plane CJFD with the main cutting edge CD.

Three-dimensional cutting can be interpreted as a collection of plane strain orthogonal cutting slices. One typical plane is represented by $IHERQGC$, which is cross-hatched in Fig. 1. This plane is defined by the cutting velocity V and the chip flow velocity vector V_c. Chip formation in this plane may be regarded as plane strain deformation with a corresponding shear angle, mean friction angle, and work material shear strength as in orthogonal cutting. Therefore, line CE may be regarded as coincident with the shear plane and line HI may be considered to be the undeformed chip thickness in orthogonal cutting. Any other plane that is parallel to the plane $IHERQGC$ will have the same effective shear plane angle ϕ_e and effective rake angle α_e, but with a different depth of cut t. Therefore, three-dimensional cutting is interpreted as a series of orthogonal slices, each with the same effective shear plane angle and effective rake angle along the main cutting edge.

The effective rake angle α_e is measured in the plane formed by the chip flow velocity V_c and cutting velocity V, and it is defined by the angle between the chip flow direction and a line normal to the cutting velocity, as shown in Fig. 1. This angle can be related to the chip flow angle (η_c), inclination angle (i), and rake angle (α_n) by [33]

$$\alpha_e = \sin^{-1}(\sin\alpha_n \cos i \cos\eta_c + \sin\eta_c \sin i) \quad (1)$$

The chip flow angle η_c can be determined by using a minimum energy approach [29,33]. The total cutting energy rate consists of the shear energy rate (U_s) on the shear plane and friction energy rate (U_f) on the tool face. The shear energy rate U_s can be expressed as:

$$U_s = \tau_s V_s A \quad (2)$$

where τ_s is the shear stress in the shear plane and V_s is the shear velocity in the shear plane. The area of the shear plane area of $CJFD$ is A, which is equal to the cross-product of the vectors $\boldsymbol{CE}$ and $\boldsymbol{CD}$, as shown in Fig. 1. An orthogonal coordinate system with origin at point C is defined as shown in this figure. The x-axis is defined along line CI and parallel to the cutting velocity vector $\boldsymbol{V}$. The y-axis is in the plane determined by $\boldsymbol{V}$ and the tool edge CD. The angle between the y-axis and line CD is i. The z-axis, not shown in Fig. 1, is perpendicular to the x- and y-axes to form a right-handed coordinate system.

The length of lines CG and HI are given by

$$CG = \frac{t_1}{\cos\alpha_n \cos\eta_c} \text{ and } HI = \frac{t_1 \cos\alpha_e}{\cos\alpha_n \cos\eta_c}.$$

Vectors $\boldsymbol{CE}$ and $\boldsymbol{CD}$ can be expressed as:

$$\boldsymbol{CE} = \left[\frac{t_1 \cos\alpha_e}{\cos\alpha_n \cos\eta_c \tan\phi_e} , \sqrt{\left(\frac{t_1 \cos\alpha_e}{\cos\alpha_n \cos\eta_c}\right)^2 - t_1^2} , \ t_1 \right]$$

and

$$\boldsymbol{CD} = [-b\tan i, b, 0]$$

The area A is equal to the cross-product $\boldsymbol{CE}\times\boldsymbol{CD}$, which can be rearranged as:

$$A = b\sqrt{t_1^2(1+\tan^2 i) + z^2} \quad (3)$$

where

$$z = \frac{p}{\tan\phi_e} + \sqrt{(p^2 - t_1^2)}\tan i \quad (4)$$

$$p = \frac{t_1 \cos\alpha_e}{\cos\alpha_n \cos\eta_c}. \quad (5)$$

Based on orthogonal cutting theory, velocity in the shear plane is given by [33]

$$V_s = \frac{\cos\alpha_e}{\cos(\phi_e - \alpha_e)} V \quad (6)$$

where ϕ_e is the angle between the shear plane and cutting velocity, and α_e is the effective rake angle. Thus, the shear energy rate U_s in Eq. (2) can be rewritten as,

$$U_s = \frac{\tau_s A \cos\alpha_e}{\cos(\phi_e - \alpha_e)} V \quad (7)$$

The friction energy rate U_f on the rake face can be found by a similar analysis [33] to be,

$$U_f = F_t \frac{\sin\phi_e}{\cos(\phi_e - \alpha_e)} V \quad (8)$$

where F_t is the friction force on the rake surface.

In order to calculate the total energy rate from Eqs. (7) and (8), the effective shear plane angle (ϕ_e) and the shear plane stress (τ_s) must be known. It is assumed

that the relationships between ϕ_e and τ_s and the effective rake angle α_e are the same as those in orthogonal cutting under equivalent conditions. In addition, by assuming that the friction force acting on a unit width of the tool face with undeformed chip thickness t is the same as the friction force in orthogonal cutting with unit width of cut and undeformed chip thickness t, the friction force F_t can be written as [29,33]:

$$F_t = \frac{\tau_s \sin\beta \cos\alpha_e}{\cos(\phi_e + \beta - \alpha_e)\sin\phi_e} Q \tag{9}$$

where β is the friction angle on the tool face, and Q for a sharp nose tool can be written as

$$Q = \frac{bt_1}{\cos i \cos\alpha_n} \tag{10}$$

Eqs. (9) and (10) are used to calculate the friction energy rate U_f.

The total cutting energy rate can be found by adding the contribution from the shear and friction energy rates. Note that the energy rates are dependent on the chip flow angle η_c, which is not known. However, the angle can be found from the condition that the chip will flow in a direction that minimizes the cutting energy U. Based on the minimum cutting energy, the tool force components can be derived from geometric considerations [33]:

$$F_H = N_t \cos\alpha_n \cos i + F_t \sin\alpha_e \tag{11}$$

$$F_V = -N_t \sin\alpha_n + F_t \cos\eta_c \cos\alpha_n \tag{12}$$

$$F_T = -N_t \cos\alpha_n \sin i + F_t \sin\eta_c \cos i - F_t \cos\eta_c \sin i \sin\alpha_n \tag{13}$$

where F_H, F_V, and F_T are the principal (cutting), vertical (thrust), and transverse components of the tool force, respectively, and N_t and F_t are the normal and friction forces that can be determined once the minimum energy is known. The force components are functions of α_n, i, b, t_1, and η_c, which are known constants, except for the chip flow angle η_c, which can be evaluated by minimizing the cutting energy. Therefore, the three-dimensional tool forces can be readily determined.

Note that in Usui's analysis [33,34], orthogonal cutting tests were necessary to provide the shear stress τ_s, shear angle ϕ_e, and friction angle β needed in the above equations. As an alternative, an Eulerian finite element cutting model is used to determine the orthogonal cutting data [29].

3. Drilling model

The analytical finite element oblique cutting technique described in the previous section is applied to selected sections along the cutting lip to determine the drilling forces. At each oblique cutting section, the three-dimensional cutting forces are calculated and then combined to determine the drilling thrust force and torque. The geometry of a typical twist drill as defined in terms of three key parameters, the helix angle, point angle (2ρ), and web-thickness ($2w$), have been presented in [1,35]. Both the helix angle and the point angle will affect the rake angle along each cutting lip. A large helix angle results in a more positive rake angle, which improves the cutting efficiency but also weakens the drill.

3.1. Cutting lip force model

For the drilling model, each cutting lip is divided into oblique cutting sections for which the corresponding three-dimensional forces can be determined. For each section, the rake and inclination angle must be determined. For straight cutting lips, the inclination angle i and normal rake angle α_n can be determined by the following formula [1]:

$$\sin i = \frac{w \sin\rho}{r} \tag{14}$$

$$\tan\alpha_n = \cos i(\tan\alpha_s \cos C_s + \tan\alpha_b \sin C_s) \tag{15}$$

where

$$\tan\alpha_s = \frac{\tan\delta}{\tan C_s} - \frac{\tan i}{\sin C_s}, \tag{16}$$

$$\cos C_s = \frac{\cos\rho}{\cos i}, \tag{17}$$

$$\tan\alpha_b = 2\pi \frac{r}{L}, \tag{18}$$

$$\delta = \tan^{-1}\left(\frac{2\pi r}{L}\right), \tag{19}$$

In these equations, w is the half web thickness, r is the radial distance from the drill axis, and L is the pitch length of the helix on the drill.

An example of the radial variation of the inclination and normal rake angles along a cutting lip of a typical twist drill with a 25.4 mm diameter, 30° helix angle, and 118° point angle is shown in Fig. 2. Note that although the normal rake angle is highly negative near the chisel edge, the inclination angle is more positive. These angles compensate for each other so that the effective rake angle remains positive or slightly negative near the chisel edge.

Using the single edge oblique cutting model, forces in the horizontal, vertical, and lateral directions can be determined. Note that forces are based on a local coordinate system for each section along each cutting lip. These local forces must be transformed to the global coordinate system corresponding to the radial, axial, and transverse directions of the drill. Forces in the axial direction contribute to the thrust force. The

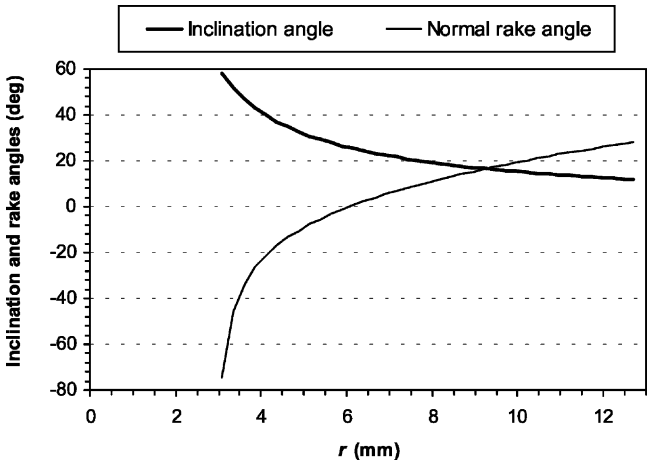

Fig. 2. Variation of normal rake and inclination angles along a cutting lip in a drill with 25.4 mm diameter, 3.07 mm half web thickness (w), 30° helix angle, and 118° point angle.

torque consists of the transverse force times the radial distance to the axis of the drill. The forces in the radial direction cancel each other due to the symmetry of the cutting lips.

Fig. 3 shows the directions of the local (F_H, F_V, F_T) forces and global force components (F_{tang}, F_{thrust}, F_{rad}) for a typical radial location along a drill cutting lip. The equations for transforming local oblique cutting forces to the global drill coordinates are:

$$F_{tang} = F_H \tag{20}$$

$$F_{thrust} = F_T \cos\rho + F_V \frac{\sqrt{(r^2 - w^2)}}{r} \sin\rho \tag{21}$$

$$F_{rad} = F_T \frac{\sqrt{(r^2 - w^2)}}{r} \sin\rho - F_V \cos\rho \tag{22}$$

Note that in general, cutting edges in a drill are curved and not necessarily straight as shown in Fig. 3. Only certain combinations of the helix angle, point angle, and radius of flute can produce a straight cutting lip.

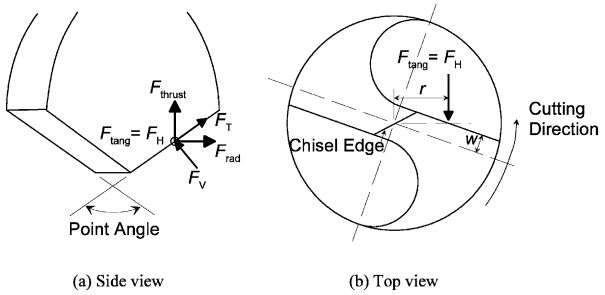

Fig. 3. Conversion of F_H, F_V, and F_T in oblique cutting to F_{rad}, F_{thrust}, and F_{tang} on a drill. (a) Side view; (b) Top view.

3.2. Chisel edge force model

The majority of the material removed by a drill occurs from the cutting action of the cutting lips. In contrast, the chisel edge provides support during drilling. Cutting along the chisel edge is not efficient due to the large negative rake angle and the slow cutting speed near the center of the drill. The cutting forces along the chisel edge typically contribute more than half of the total thrust force, while only contributing a very small portion of the drilling torque. Although the chisel edge removes little material, it plays an important role in providing drill point strength to resist lateral bending moments due to vibration or unbalanced forces during drilling.

Cutting within the chisel edge region can be treated as equivalent orthogonal cutting slices. The cutting speed for each slice depends on the distance from the centerline. The cutting speed varies from nearly zero at the center of the drill to its maximum at the transition with the cutting lip.

For a typical drill with a 118° point angle, the rake angle for an orthogonal section in the web region is −59°. Cutting under such a negative rake angle is very difficult to model with an updated-Lagrangian finite element formulation [36]. However, an Eulerian approach can be successfully applied for orthogonal cutting with large negative rake angles, as long as the mesh is carefully designed.

An example of a mesh for orthogonal cutting with a −59° rake angle is shown in Fig. 4. Both the workpiece and the cutting tool are included in the Eulerian model. The strain-rate in the shear zone of cutting with –59°

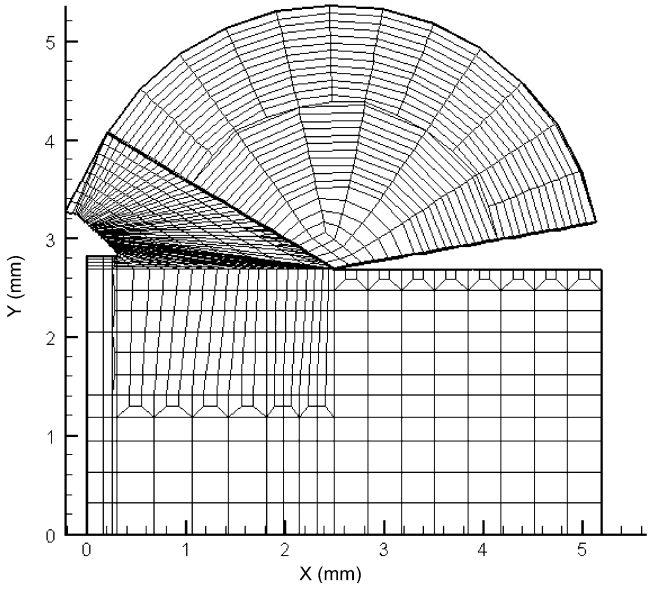

Fig. 4. Finite element mesh for a –59° negative rake angle for the web of a drill with 118° point angle.

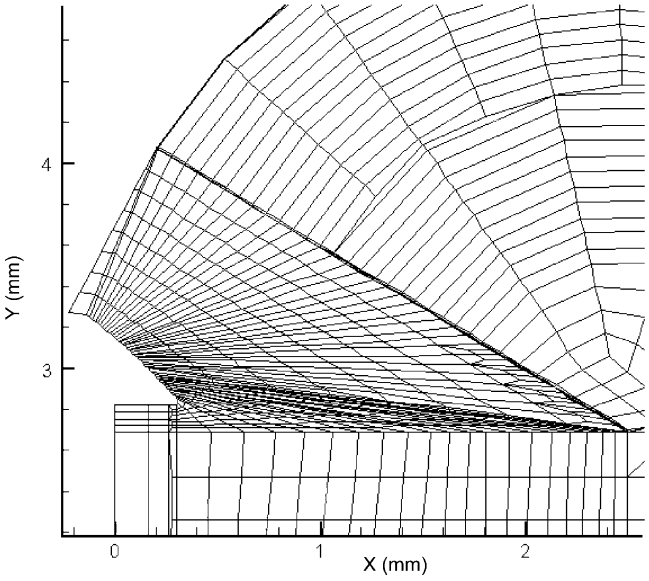

Fig. 5. Close-up view of the finite element mesh.

rake angle is about 300 s^{-1}, which is much smaller than the 6000 s^{-1} strain-rate for cutting with a positive rake angle. A close-up view of the mesh in the shear zone is shown in Fig. 5. Note that a thin layer of elements is included to model shear deformation along the tool-chip interface. The temperature gradient across this layer can be used to estimate the heat flux that occurs between the chip and the tool rake face.

4. Experimental validation

The finite element model used to determine the cutting forces in drilling is validated using three sets of cutting tests. These include orthogonal cutting, oblique cutting, and drilling. For all the tests, a Kistler model 9255B three-axis piezoelectric force dynamometer was used to measure the cutting and drilling thrust forces.

4.1. Orthogonal cutting

Orthogonal cutting tests were performed on a conventional lathe on an AISI 1020 carbon steel tube with a 76.2 mm outside diameter and 3.18 mm wall thickness. In the orthogonal cutting tests, precisely ground high speed steel tools with six rake angles of –30, –15, 0, 10, 20, and 30° were used. All the tools had a clearance angle of 10°.

The measured principal (cutting) and vertical (thrust) forces, F_H and F_V, for the orthogonal cutting tests are shown for two feeds of 0.094 and 0.13 mm/rev in Figs. 6 and 7, respectively. These tests were conducted at a cutting speed of 0.42 m/s. The cutting and thrust forces predicted by the finite element model are represented by open circles. As expected, larger cutting and thrust forces were obtained for the smaller rake angles for both feeds. The higher feed (0.13 mm/rev) also generated larger cutting and thrust forces. In general, the measured cutting forces agreed well with the predicted forces, as shown in Figs. 6 and 7. The bars in these figures indicate the experimental variation in the measured forces. The favorable agreement between the measured and computed tool forces justified their use in the oblique cutting models.

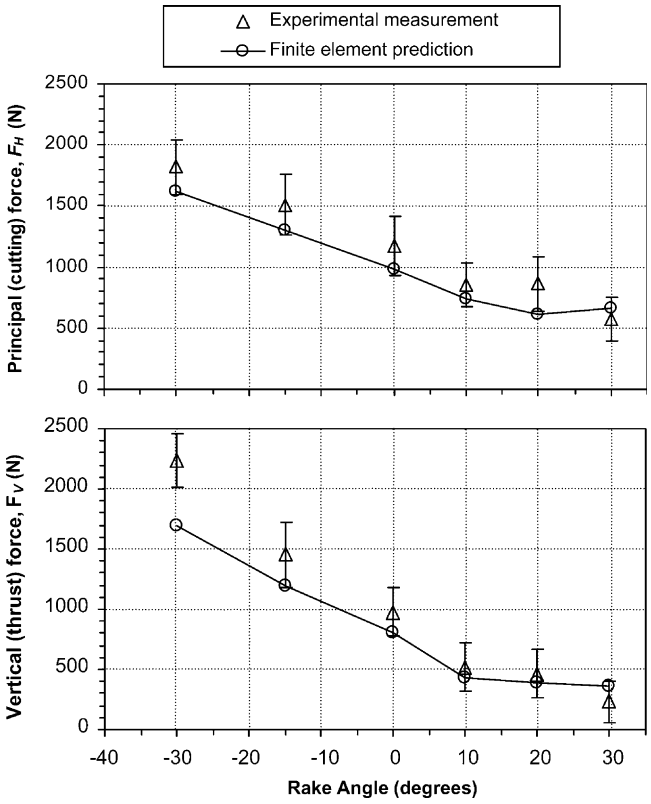

Fig. 6. Comparison of finite element predicted and measured principal (cutting) and vertical (thrust) forces in orthogonal cutting for 0.094 mm/rev feed for six rake angles.

4.2. Oblique cutting

The same AISI 1020 tube and lathe were used in the oblique cutting experiments. A zero degree rake angle was used with five inclination angles of 5, 15, 25, 35, and 45°. Three components of the cutting forces, F_H, F_V, and F_T, were measured using a three-axis force dynamometer and these forces were then compared with the finite element calculated forces.

Fig. 8 shows a comparison between the measured and finite element predicted oblique cutting forces for a 0.13 mm/rev feed and a 0.80 m/s cutting speed. In general, good agreement was found between the measured and computed forces for all five inclination angles. Note that the bars indicate the variation in the measured forces.

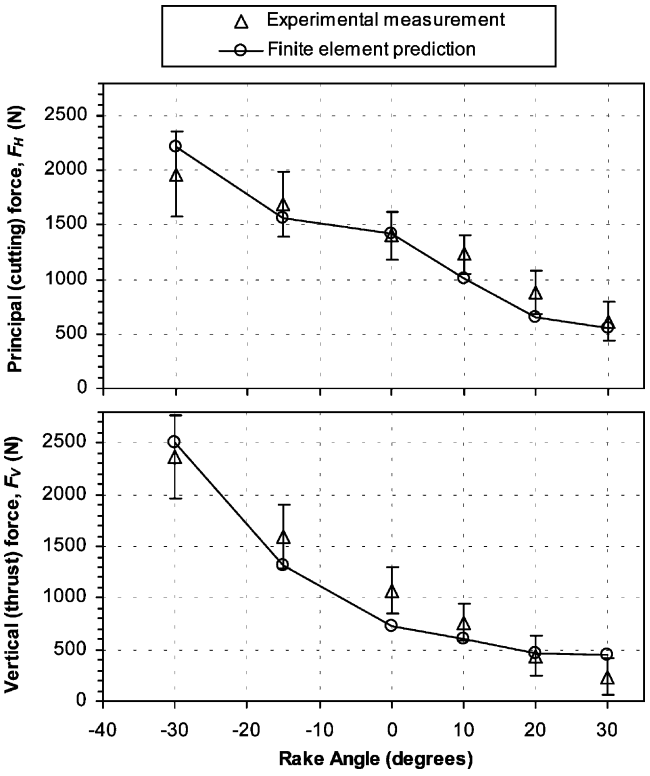

Fig. 7. Comparison of finite element predicted and measured principal (cutting) and vertical (thrust) forces in orthogonal cutting for 0.13 mm/rev feed for six rake angles.

4.3. Drilling

The drilling tests were performed on a Bridgeport milling machine using a high speed steel twist drill with a 3.2 mm web thickness, 30° helix angle, and 118° point angle. The workpiece was an AISI 1020 steel block. A spindle speed of 302 rpm was used. Three drills with 6.35, 9.53, and 12.5 mm diameters were used for three feed rates of 0.051, 0.076, and 0.102 mm/rev.

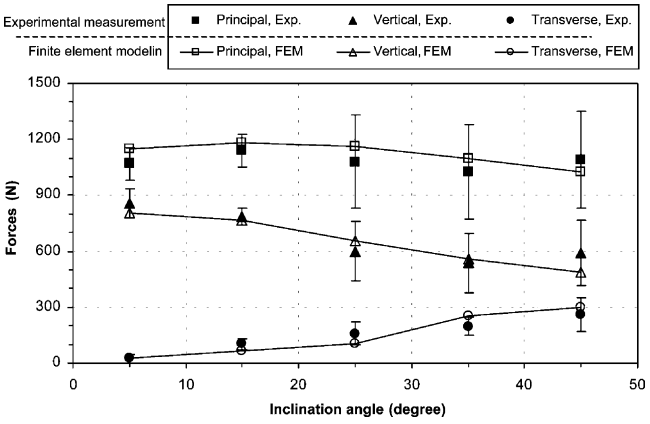

Fig. 8. Comparison of finite element predicted and measured cutting, thrust, and transverse forces for 0.13 mm/rev feed, 0.80 m/s cutting speed, and five inclination angles.

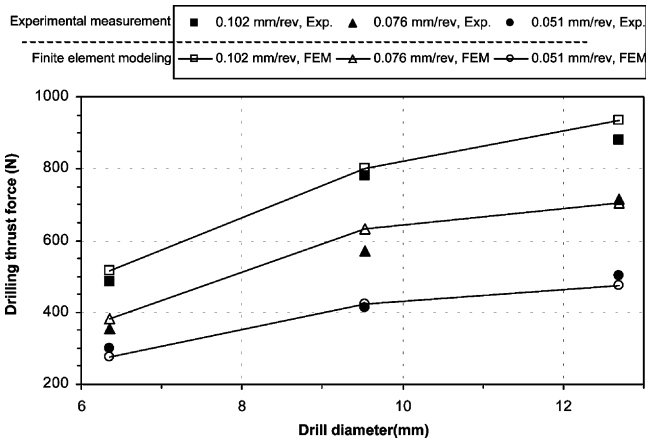

Fig. 9. Comparison of finite element predicted and measured thrust force in nine drilling tests.

A comparison of the measured and predicted thrust forces is shown in Fig. 9. Very good agreement for the drilling thrust force was observed. As expected, a larger thrust force occurred for larger diameter drills and higher feed rates.

A drilling torque dynamometer was not available to directly measure the torque. However, the same cutting force components that comprise the thrust force are also used to calculate the torque. Therefore, it is reasonable to assume that since good agreement was found between the measured and predicted thrust forces, good agreement would also occur between the measured and predicted torque. As an alternative, the predicted torque was compared with measured torque as reported by Rubenstein [18] for drilling of AISI 1020 steel. The thrust and torque for drilling with three drills with diameters of 6.35, 9.53, and 12.7 mm were reported. These drills had a 27° helix angle, 120° point angle, 0.30 m/s peripheral drill speed, and a 0.102 mm/rev feed rate. Since a two-flute drill was used, the depth of cut in the finite element model is half of the feed per revolution or 0.051 mm. Table 1 shows a comparison between the predicted and measured torque and thrust forces. The good agreement between the measured and predicted values for both the thrust force and torque further validates the

Table 1
Comparison of predicted and measured thrust force and torque

Drill diameter (mm)	Torque (N·m)		Thrust force (N)	
	FEM model	Experimental measurement [18]	FEM model	Experimental measurement [18]
6.35	1.61	1.81	735	775
9.53	3.47	3.51	1040	1070
12.7	6.17	5.88	1380	1440

Table 2
Sections of oblique cutting for drilling with 12.7 mm diameter, 30° helix angle, 118° point angle, 1.70 mm web thickness, and 302 rpm spindle speed

r (mm)	Cutting speed, V (mm/s)	Depth of cut, t_1 (mm)	Width of cut (mm)	Inclination angle, i (°)	Rake angle, α_n (°)	Chip flow angle, η_c (°)	Effective rakeangle, α_e (°)	F_{tang} (N)	F_{rad} (N)	F_{thrust} (N)	Torque, $F_{tang}r$ (N·mm)
5.82	183.9	0.051	1.04	7.7	28.3	1	28.2	95.1	30.2	39.6	554
4.78	151.1	0.051	1.04	8.8	22.3	4	22.9	100	32.9	40.4	476
3.73	118.1	0.051	1.04	11.3	15.1	6	16.0	107	36.1	43.9	398
2.69	85.1	0.051	1.04	15.7	6.0	11	8.7	118	42.0	49.3	318
1.63	51.3	0.051	1.04	26.6	−8.6	21	2.0	143	57.3	57.0	233
0.97	30.5	0.051	0.28	0	−59.0	0	−59.0	35.9	0.0	64.5	34.8
0.69	21.6	0.051	0.28	0	−59.0	0	−59.0	35.9	0.0	64.5	24.8
0.41	13.0	0.051	0.28	0	−59.0	0	−59.0	35.9	0.0	64.5	14.7
0.14	4.3	0.051	0.28	0	−59.0	0	−59.0	35.9	0.0	64.5	5.03

analytical finite element drilling technique described in this paper.

In the finite element model, five sections were used to represent each cutting lip and four sections were used to model the chisel edge. Table 2 lists the geometry of each section for a twist drill with a 12.7 mm diameter, 30° helix angle, 118° point angle drill, 1.70 mm web thickness, and 302 rpm spindle speed. For each section, the table lists the radial location of the section, the cutting speed, depth of cut, width of cut, inclination angle, rake angle, chip flow angle, and effective rake angle. Note that from the outer to the inner drill radius, the effective rake angle decreases and the inclination angle increases for each section which indicates that the cutting action is becoming more oblique. Throughout the chisel edge region, orthogonal conditions are in effect so that the inclination angle is zero and the rake angle has a large negative value. For drilling of AISI 1020 steel, the forces for each section are also shown in this table. As expected, the radial force F_{rad} is zero in the chisel edge region

5. Conclusions

A three-dimensional drilling model has been described for determining the thrust force and torque in drilling. The model is applicable to general drill geometries, as characterized by the point and flute geometry, under different workpiece material and cutting conditions. The predicted forces can be readily coupled with solids models, so that complex drill geometries can be accurately represented. Because the technique described is independent of any specific drill geometry, it can be readily applied to non-conventional drills other than standard twist drills. Other applications of the technique include drill design and selection for high speed and dry drilling.

This technique can be extended to predict drill tip temperatures, which is an important indicator of drill life and drilling performance. Research has been conducted [37] in which the heat flux from each oblique and orthogonal section can be determined and then applied to calculate the temperature distribution throughout the drill, including the cutting lip and chisel edge regions where temperatures are the highest. In addition, a new temperature measurement method [38] offers a new opportunity to measure the temperature distribution along the cutting edges of a drill.

References

[1] M.C. Shaw, Metal Cutting Principles, third ed., M.I.T., Cambridge, Mass., 1954.
[2] C.J. Oxford, On the drilling of metals I—basic mechanics of the process, Transactions of ASME 77 (1955) 103–114.
[3] M.C. Shaw, C.J. Oxford, On the drilling of metals II—the torque and thrust of drilling, Transactions of ASME 79 (1957) 139–148.
[4] A.K. Pal, A. Bhattacharyya, G.C. Sen, Investigation of the torque in drilling, International Journal of Machine Tool Design and Research 4 (1965) 205–221.
[5] R.A. Williams, A study of the basic mechanics of the chisel edge of a twist drill, International Journal of Production Research 8 (1970) 325–343.
[6] R.A. Williams, A study of the drilling process, Journal of Engineering for Industry 96 (1974) 1207–1215.
[7] E.J.A. Armarego, C.Y. Cheng, Drilling with flat rake face and conventional twist drills—I. theoretical investigation, International Journal of Machine Tools and Manufacture 12 (1972) 17–35.
[8] E.J.A. Armarego, C.Y. Cheng, Drilling with flat rake face and conventional twist drills—II. experimental investigation, International Journal of Machine Tools and Manufacture 12 (1972) 37–54.
[9] S. Wiriyacosol, E.J.A. Armarego, Thrust and torque prediction in drilling from a cutting mechanics approach, Annals of CIRP 28 (1979) 88–91.
[10] A.R. Watson, Drilling model for cutting lip and chisel edge and comparison of experimental and predicted results. I—initial cutting lip model, International Journal of Machine Tool Design and Research 25 (1985) 347–365.
[11] A.R. Watson, Drilling model for cutting lip and chisel edge and comparison of experimental and predicted results. II—reversed cutting lip model, International Journal of Machine Tool Design and Research 25 (1985) 367–376.

[12] A.R. Watson, Drilling model for cutting lip and chisel edge and comparison of experimental and predicted results. III—drilling model for chisel edge, International Journal of Machine Tool Design and Research 25 (1985) 377–392.
[13] A.R. Watson, Drilling model for cutting lip and chisel edge and comparison of experimental and predicted results. IV—drilling tests to determine chisel edge contribution to torque and thrust, International Journal of Machine Tool Design and Research 25 (1985) 393–404.
[14] J.S. Agapiou, M.F. DeVries, On the determination of thermal phenomena during a drilling process—part I, analytical models of twist drill temperature distributions, International Journal of Machine Tools and Manufacture 30 (1990) 203–215.
[15] J.S. Agapiou, M.F. DeVries, On the determination of thermal phenomena during a drilling process—part II, comparison of experimental and analytical twist drill temperature distributions, International Journal of Machine Tools and Manufacture 30 (1990) 217–226.
[16] D.A. Stephenson, J.S. Agapiou, Calculation of main cutting edge forces and torques for drills with arbitrary point geometries, International Journal of Machine Tools and Manufacture 32 (1992) 521–538.
[17] C. Rubenstein, The torque and thrust force in twist drilling—I. theory, International Journal of Machine Tools and Manufacture 31 (1991) 481–489.
[18] C. Rubenstein, The torque and thrust force in twist drilling—II. comparison of experimental observations with deductions from theory, International Journal of Machine Tools and Manufacture 31 (1991) 491–504.
[19] V. Chandrasekharan, S.G. Kapoor, R.E. DeVor, A mechanistic approach to predicting the cutting forces in drilling: with application to fiber-reinforced composite materials, Journal of Manufacturing Science and Engineering 117 (1995) 559–570.
[20] V. Chandrasekharan, S.G. Kapoor, R.E. DeVor, A mechanistic model to predict the cutting force system for arbitrary drill point geometry, S.M. Wu Symposium, 2 (1996) 108–114.
[21] V. Chandrasekharan, S.G. Kapoor, R.E. DeVor, A mechanistic model to predict the cutting force system for arbitrary drill point geometry, Journal of Manufacturing Science and Engineering 120 (1998) 563–570.
[22] Y. Gong, K.F. Ehmann, Mechanistic model for dynamic forces in micro-drilling, Proceedings of 2001 ASME International Mechanical Engineering Congress and Exposition, Nov. 11–16, 2001, New York, NY, MED-23302 (2001).
[23] K.H. Fuh, Computer Aided Design and Manufacturing of Multi-Facet Drills, PhD Dissertation, University of Wisconsin at Madison, 1987.
[24] Y. Guo, D.A. Dornfeld, Finite element analysis of drilling burr minimization with a backup material, Transaction of the North American Manufacturing Research Institution of SME 26 (1998) 207–212.
[25] S. Min, D.A. Dornfeld, J. Kim, B. Shyu, Finite element modeling of burr formation in metal cutting, Machining Science and Technology 5 (2001) 307–322.
[26] M. Shatla, T. Altan, Analytical modeling of drilling and ball end milling, Journal of Materials Processing Technology 98 (2000) 125–133.
[27] M. Bono, J. Ni, The effects of thermal distortions on the diameter and cylindricity of dry drilled holes, International Journal of Machine Tools and Manufacture 41 (2001) 2261–2270.
[28] M. Bono, J. Ni, A model for predicting the heat flow into the workpiece in dry drilling, Journal of Manufacturing Science and Engineering 124 (2002) 773–777.
[29] J.S. Strenkowski, A.J. Shih, J.C. Lin, An analytical finite element model for predicting three-dimensional tool forces and chip flow, International Journal of Machine Tools and Manufacture 42 (2002) 723–731.
[30] J.T. Carroll, J.S. Strenkowski, Finite element models of orthogonal cutting with applications to single point diamond turning, International Journal of Mechanical Science 30 (1988) 899–920.
[31] J.S. Strenkowski, K.J. Moon, Finite element prediction of chip geometry and tool/workpiece temperature distributions in orthogonal cutting, Journal of Engineering for Industry 112 (1990) 313–318.
[32] S. Athavale, J.S. Strenkowski, Material damage-based model for predicting chip-breakability, Journal of Manufacturing Science and Engineering 119 (1997) 675–680.
[33] E. Usui, A. Hirota, M. Masuko, Analytical prediction of three dimensional cutting process: part 1 basic cutting model and energy approach, ASME Journal of Engineering for Industry 100 (1978) 222–228.
[34] E. Usui, A. Hirota, Analytical prediction of three dimensional cutting process: part 2, chip formation and cutting force with conventional single-point tool, ASME Journal of Engineering for Industry 100 (1978) 229–235.
[35] M.C. Shaw, Metal Cutting Principles, Oxford University Press, London, 1984.
[36] A.J. Shih, Finite element analysis of the rake angle effects in orthogonal metal cutting, International Journal of Mechanical Sciences 38 (1996) 1–17.
[37] Hsieh, C.C. (1998) Development of a force and temperature twist drill model for AISI 1020 steel, PhD Dissertation, North Carolina State University.
[38] M. Bono, J. Ni, A method for measuring the temperature distribution along the cutting edges of a drill, Journal of Manufacturing Science and Engineering 124 (2002) 921–923.